Validation of IASI L2Pcore Sea Surface Temperature

Doc.No.	:	EUM/MET/DOC/10/0472
Issue	:	v1A
Date	:	23 March 2011

EUMETSAT
Eumetsat-Allee 1, D-64295 Darmstadt, Germany
Tel: +49 6151 807-7
Fax: +49 6151 807 555
http://www.eumetsat.int

Document Change Record

Issue / Revision	Date	DCN. No	Changed Pages / Paragraphs
v1	8 Mar 2011		First issue.
v1A	23 Mar 2011		Editorial updates.

Table of Contents

1 INTRODUCTION

1.1 Purpose and Scope

The first Metop satellite was launched in October 2006 [RD 1] with payloads which include ATOVS, AVHRR, IASI, GOME-2, ASCAT and GRAS. The IASI instrument provides sounding data of temperature, water vapour and ozone monitoring. Additionally, retrievals of sea surface temperature (SST) are possible from IASI.

Retrievals of surface skin temperature over land and sea have been provided by the Infrared Atmospheric Sounding Interferometer (IASI) L2 Product Processing Facility (PPF) at EUMETSAT since April 2008. These data are available via EUMETCast with vertical temperature and humidity profiles [RD 2]. The IASI skin SSTs have been previously validated against AATSR SST and ECMWF fields to have a cool bias of around 0.4 K and standard deviation of 0.4 K [RD 3].

Plans are in place to produce the IASI SST data in GHRSST L2P format at EUMETSAT, to be consistent with other SST data providers. The values of the SSTs are the same as those in the IASI L2 PPF. Validation results of this new product show that the IASI SSTs are of good quality, but have a mean cool bias of around 0.4 K. A Single Sensor Error Statistic (SSES) scheme has been developed for the IASI SSTs based on water vapour profiles contained within the IASI L2 product. An experimental L2Pcore product containing SST, SSES and quality levels has been produced at EUMETSAT since March 2010. The results are presented with a description of the work involved to produce the Single Sensor Error Statistics.

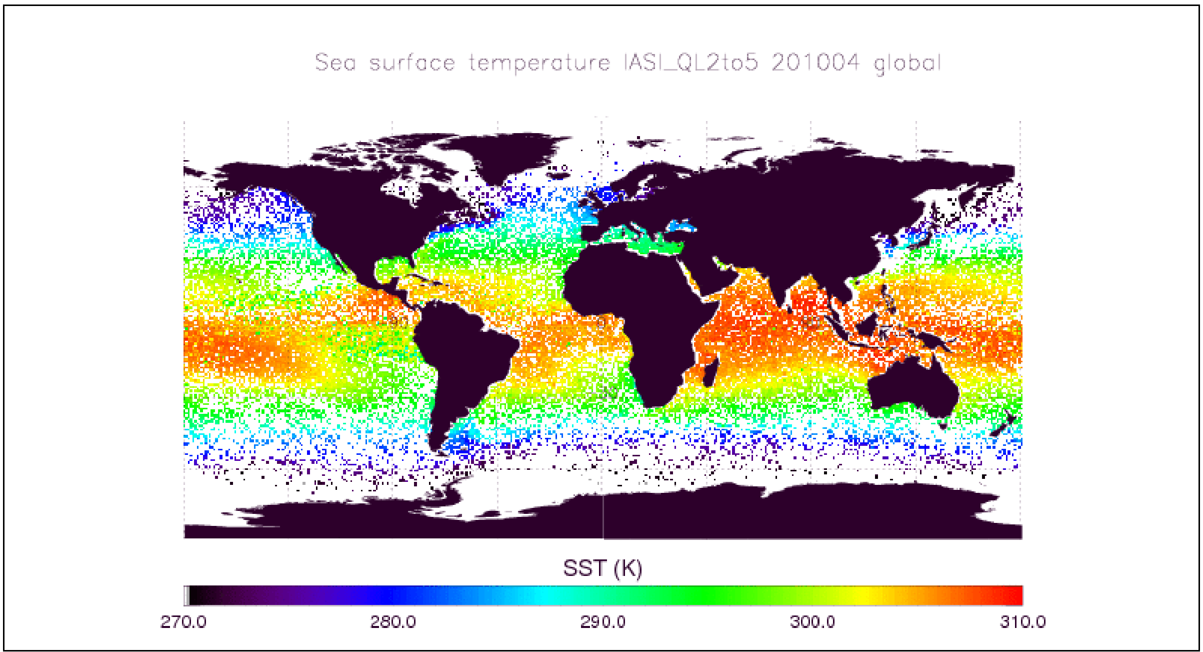

Figure 1: IASI L2Pcore SST April 2010

The report includes an overview of the IASI SSES scheme, validation results, and details of future progress towards the operational availability of the IASI L2Pcore SST product. Figure 1 shows a global plot of the IASI L2Pcore SST for April 2010.

1.2 Document Structure

The document firstly gives an overview of SST from IASI in Section 2; followed by the drifting buoy validation results in Section 3 and checks on the conformity of operational product implementation in Section 4; finally conclusions and way forward are discussed in Section 5.

2 SEA SURFACE TEMPERATURE FROM IASI

2.1 IASI L2Pcore

IASI L2Pcore datasets comply with the GHRSST Data Specification 2.0 [RD 4], and are provided in netCDF4 format. They contain the ‘core’ fields of: latitude, longitude, delta time from reference time, SST, SSES, quality level and L2P flags. In addition, wind speed is provided from ECMWF 10-metre forecast fields, enabling users to assess the likelihood of large diurnal variations influencing the observations. The SST retrieved from IASI is a ‘skin’ SST measurement, representative of the temperature of the ocean in the top few millimetres. The IASI L2Pcore is a swath product available in near-real time, and the resolution of the IASI IFOV is 0.01465 radians [RD 2].

Sea surface temperature retrieved from the IASI instrument should be seen as a long-term and stable contribution to the SST global observing system, due to the committed continuity of this instrument upon the Metop series of satellites (up to 2023), and infrared sounding instruments planned for Post-EPS and MTG-S enabling data coverage up to the early 2030’s and beyond [RD 5]. Climate research requires SST long-term datasets of greater than 15 years [RD 6]. It is important that datasets are consistently reprocessed throughout, and ideally have an overlap period between sensors for correct characterisation. The IASI spatial resolution is lower than that of other infrared SST sensors such as AVHRR or AATSR, but it is important that a range of SSTs from different sensors are available so that FCDRs are able to fully utilise respective strengths of each instrument, and for the understanding of the errors and biases between observations. In addition, SST retrieved from IASI has the potential for improved atmospheric correction over other sensors using commonly used multi-spectral retrieval techniques.

2.2 Single Sensor Error Statistics

A major error contribution in infrared SST retrievals is the amount of water vapour in the atmosphere [RD 7]. The SSES scheme developed for IASI SST observations uses integrated water vapour derived from the IASI water vapour profiles contained in the IASI L2 product. IASI is uniquely placed to utilise this information to gain information on the observational errors.

To investigate possible relationships between IASI water vapour profiles and the quality of the SST retrieval, differences between IASI and climatology SSTs (NSIPP monthly climatology, [RD 8]) were plotted against integrated water vapour (IWV). IWV was calculated by integrating the IASI water vapour profiles (kg/kg) with pressure level information. Figure 2 shows a plot of IASI minus climatology SST versus IWV. The SSTs with the smallest biases and error bars occur between 0 and 1.5 IWV. The largest deviations are where IWV is less than 0.5, due to two observations where the climatology is reporting an ice surface temperature, whilst the IASI SST measures a sea temperature.

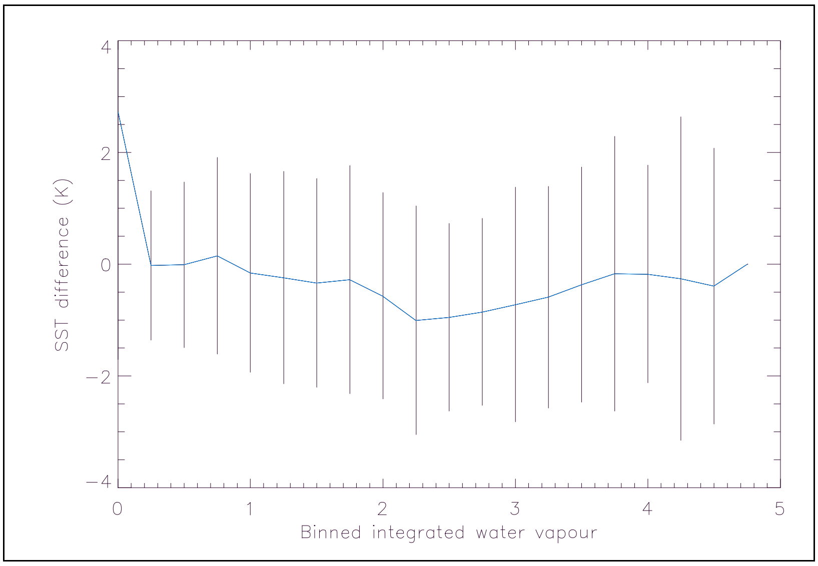

Figure 2: IASI minus climatology SST differences versus IASI integrated water vapour 1 November 2008

Thresholds have been determined from Figure 2 to give quality levels ranging from 2 (worst usable data) to 5 (best). The thresholds have been applied to Metop/AVHRR level 3 data. Figure 3 shows IASI minus AVHRR (L3) differences for 1 November 2008, separated according to quality level. The 'best' quality observations, level 5, show the smallest bias and standard deviation of -0.53 K and 0.47 K respectively. With decreasing quality level, the standard deviations increase. The figure indicates that the IWV thresholds chosen create an effective way of stratifying the errors according to quality level.

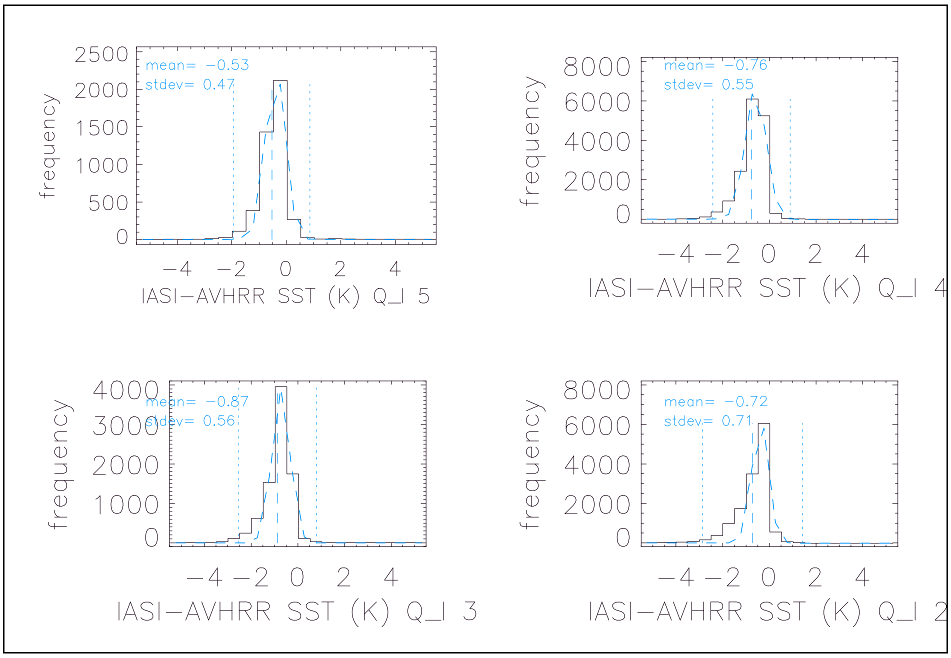

Figure 3: IASI minus AVHRR histograms for quality levels 2 to 5 for 1 November 2008

Figure 4 shows the global spread of quality levels from 2 to 5 for IASI L2Pcore data from April 2010. The quality levels are seen to represent different water vapour regimes, which follow different error characteristics.

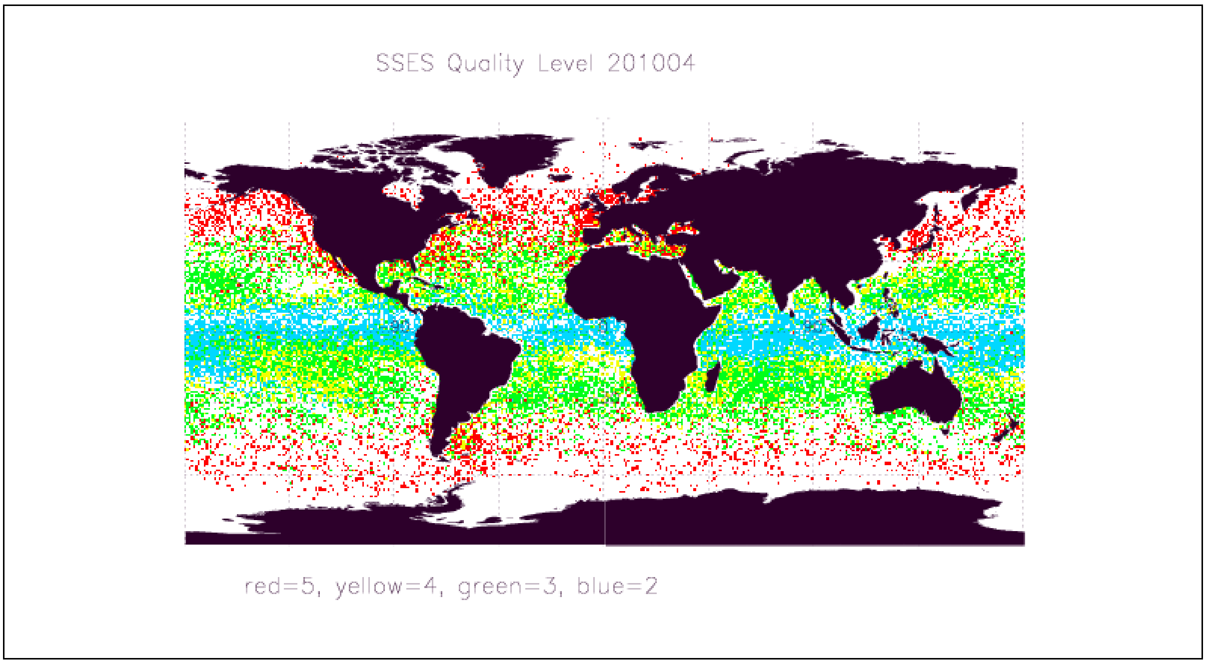

Figure 4: IASI L2P core SSES quality levels for April 2010

2.3 IASI Multi-Matchup Dataset

In order to assess the quality of the IASI SST retrievals, a multi-matchup dataset (MMD) was compiled to create a dataset containing collocated IASI, AVHRR and drifting buoy SSTs. A matchup dataset (MDB) of AVHRR L2P and *in situ* SSTs [RD 8] was supplied by the OSI-SAF. Each AVHRR/*in situ* measurement was collocated to the nearest IASI SST observation using the following criteria:

- The AVHRR and IASI observations must be within an hour of each other.
- The latitude and longitude distances between AVHRR and IASI are within 0.12 degrees. This retains an AVHRR and drifting buoy observation within the central half of the IASI IFOV.
- Only drifting buoy observations were used.
- The IASI and drifting buoy SSTs must be within valid ranges.
- An extreme-gross check that the absolute value of drifting buoy minus IASI SST must be less than 20 K.

The IASI observations are collocated to the AVHRR observations, recording the corresponding drifting buoy observations. No checks are performed between the AVHRR and buoy SSTs, therefore the criteria to build the MMD for these observations is that used by the OSI-SAF [RD 8].

3 DRIFTING BUOY VALIDATION

3.1 Global Statistics and SSES Derivations

The IASI MMD has been used to analyse global statistics of IASI SST, AVHRR SST and drifting buoy SST observations. These statistics have been analysed per IASI quality level to determine the SSES bias and standard deviations to be applied to future IASI L2P data. In addition to the criteria outlined in Section 2.3, further quality control was applied during the calculation of the SSES. These further tests are outlined in Table 1 below. The table also describes how the tests for the regional analyses (Section 3.3) vary in order to retain a significant number of collocations to derive statistics. During the calculation of the statistics the OSI-SAF buoy black list information [RD 9] was used to exclude anomalous buoy SSTs. The IASI skin SSTs were converted to a sub-skin SST by the addition of 0.17 K [RD 10]. Three-sigma error statistics were calculated throughout, in order to exclude outliers, for the statistics tables and time-series; however, the plots and maps elsewhere in the report contain the whole distribution.

Criterion name	Analyses applied	Description of quality control	Comment
GHRSST_check	All	IASI SST observation must have occurred within ±2 hours of the drifting buoy observation.	This aligns with current GHRSST guidelines, but may be reduced to 1 hour in future as increased collocations are obtained.
	All	Night-time only observations.	To reduce diurnal variation effects.
Distance_check	All	Location of buoy checked to be within IASI IFOV.	Due to constraint of collocating AVHRR with IASI for the MDB, the distance between IASI and buoy is much less than the IFOV radius.
Gross_check	SSES; global	Satellite SSTs are checked to be within valid ranges.	
	SSES; global	Drifting buoy and IASI SST observations are checked to be within 5 K of climatology.	OSI-SAF MDB climatology used.
QL3_check	SSES; global; regional	Only AVHRR observations with a quality level of 3 or higher are used.	Regional analyses include these checks but exclude gross_check and stdev_check in order to retain a significant number of collocations.
Stdev_check	SSES; global	The standard deviation of the AVHRR SSTs over a 21x21 box must be less than or equal to 0.3 K.	The 21x21 box encompasses an approximation of the IASI IFOV.

Table 1: Description of collocation criteria applied to buoy, IASI, AVHRR SST statistics derivation

Table 2 presents the SSES bias and standard deviations derived from the MMD covering the period 1 April to 30 September 2010 (a six-month period to align with GHRSST guidelines for the derivation of SSES). These SSES values are included within the IASI L2Pcore products from December 2010 onwards. The standard deviations for all quality levels are less than 0.5 K, and are similar for all quality levels. The largest standard deviation is observed for the lowest quality level data (2), whilst the highest bias is observed for the quality level 3 data. For the non-3-sigma statistics (in brackets) the pattern of higher quality level results (5) displaying the smallest bias and lowest standard deviation is seen clearly, indicating that outliers affect the SSTs for non-robust statistics. The IASI SSTs show a cool bias with respect to the drifting buoy SSTs, indicating that perhaps some residual cloud contamination remains. Figure 5 shows a time-series of the monthly SSES bias and standard deviations through the six-month period. The red curves, displaying the 'best' quality level 5 results, are generally the lowest in bias and standard deviation, with some monthly variation.

Quality level	SSES bias (K)	SSES stdev (K)
2	-0.24 (-0.30)	0.42 (0.67)
3	-0.46 (-0.52)	0.35 (0.58)
4	-0.39 (-0.45)	0.36 (0.47)
5	-0.34 (-0.36)	0.41 (0.43)

Table 2: Global statistics of IASI L2Pcore MDB per quality level for 1 April to 30 September 2010; 496 (512) collocations

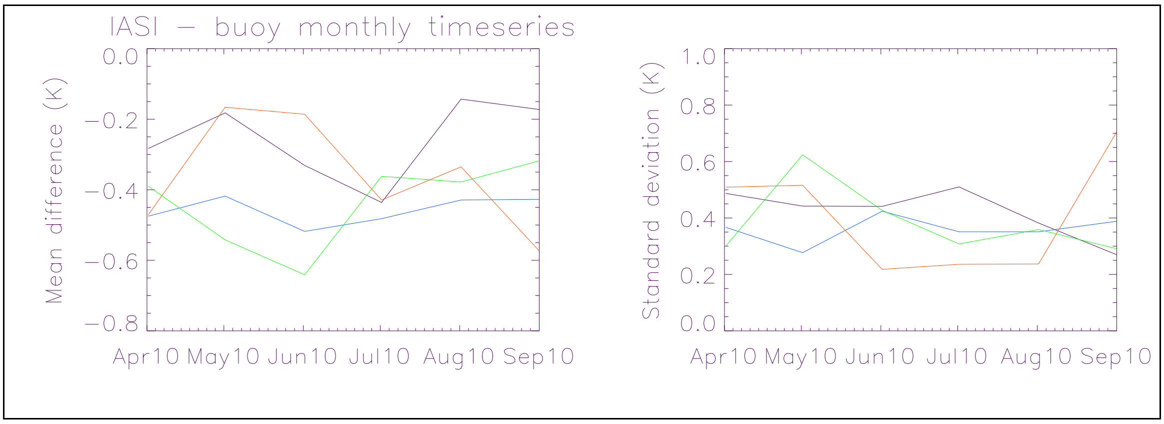

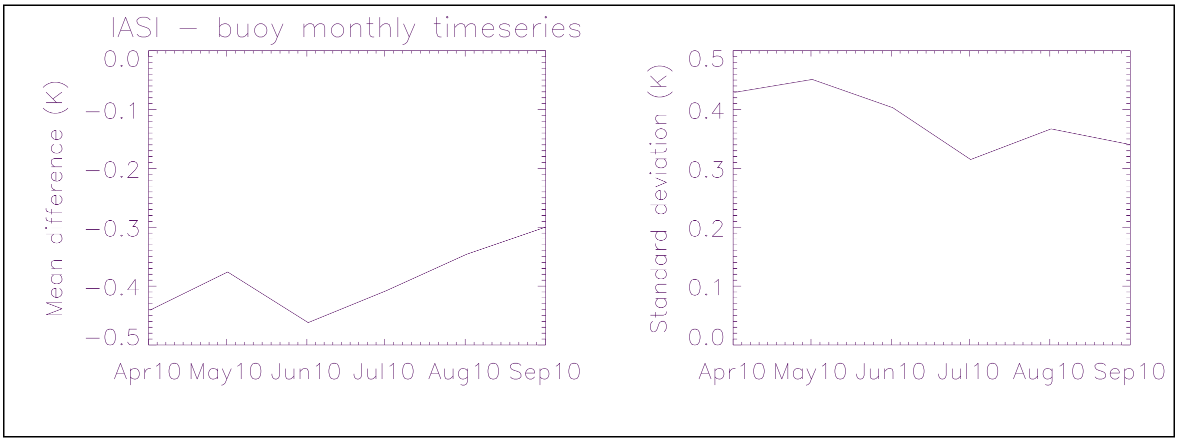

Figure 5: a) (top) Time-series of IASI SST SSES bias and standard deviation from April to September 2010 (red=quality level 5; green=4 ; blue=3 ; black=2); b) (lower) Time-series of IASI SST SSES bias and standard deviation from April to September 2010 for all SSTs

Global analyses for all quality levels, with the same matchup criteria, give the mean IASI minus buoy difference as -0.40 K, with a standard deviation of 0.40 K. For the same collocations, the mean AVHRR minus IASI difference is 0.43 K, with a standard deviation of 0.38 K. These results support the conclusion that a cool bias remains in the IASI SSTs, with the AVHRR SSTs unbiased with respect to *in situ* observations. Histograms of IASI minus buoy SST differences in Figure 6 for each quality level show a cool tail, most likely due to residual cloud contamination in the IASI SST data. The cool tail is most apparent in the lowest quality level results (2).

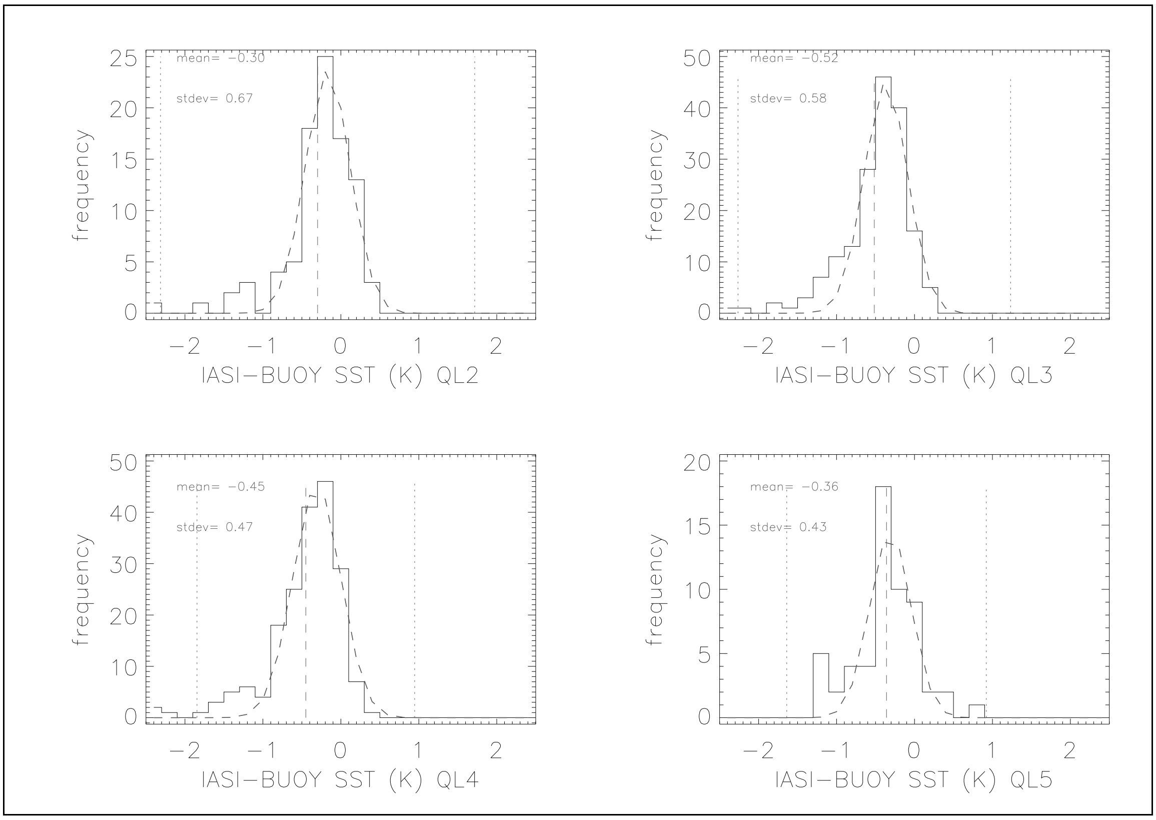

Figure 6: Histograms of IASI minus buoy differences for 1 April to 30 September 2010 for quality levels 2 to 5

Figure 7 shows a global map of IASI minus drifting buoy differences for April to September 2010. The largest deviations are in regions typically affected by aerosol such as off the West African coast and the Arabian Sea. Additionally, some occasional red points are observed which are likely to be due to residual cloud contamination causing cool IASI SSTs.

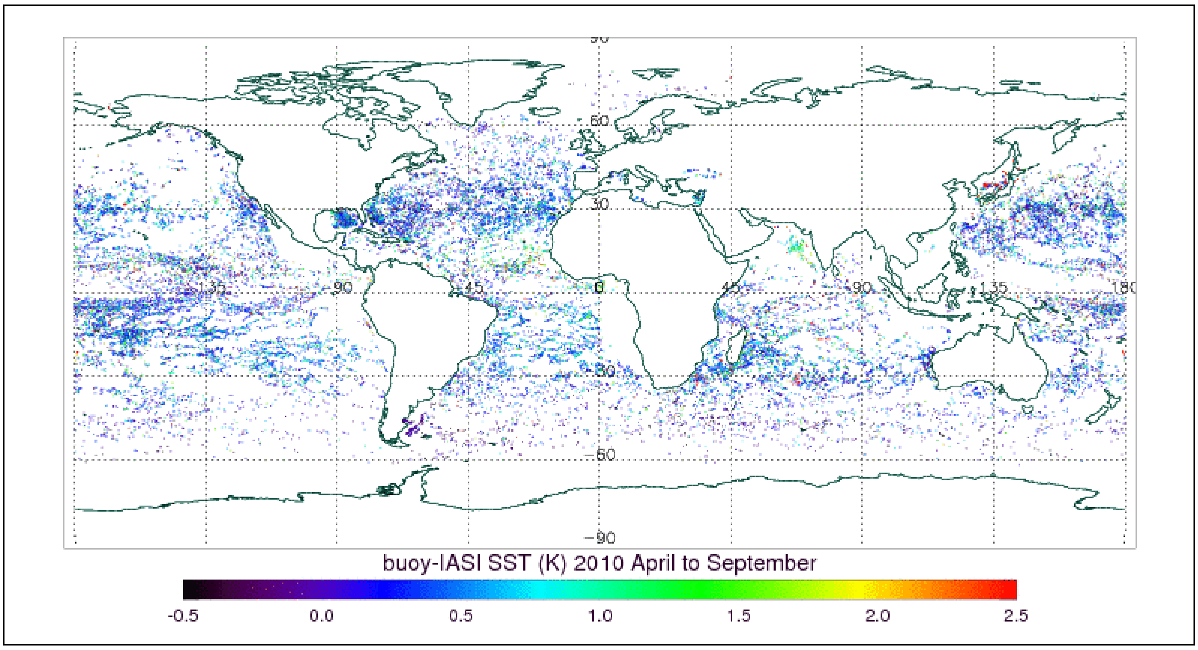

Figure 7: Global map IASI minus drifting buoy SST for April to September 2010

To look at the impact of day-time SSTs on IASI bias, statistics were analysed using the same criteria: QL3_check, distance_check, and the GHRSST_check (but alternating day for night observations) for the whole six-month period. The night-time statistics gave the IASI minus buoy SST mean difference as -0.4 K, standard deviation 0.46 K (1698 collocations); and the day-time statistics gave the mean difference as -0.25 K, standard deviation 0.44 K (2078 collocations). Therefore the diurnal variations in the IASI day-time SSTs have the effect of reducing the bias, by warming the SSTs by 0.15 K.

3.2 Three-way Error Statistics

Given three independent collocated SST observation sources, it is possible to estimate the uncertainties on each observation type, using the method described in [RD 11]. An important assumption for using this method is that the errors between the observations are uncorrelated. It is assumed that this assumption is applicable in this case because the IASI and AVHRR SSTs have completely independent retrieval schemes, and are independent of drifting buoys. Additionally, the covariances between the different observations due to representativity must be negligible. The method has also been used to ascertain errors of other ocean observations such as wind [RD 12] and wave [RD 13], and the method is being tested on sea-ice drift [RD 14].

In order to test the assumption that the errors between the observations are uncorrelated, the MMD was analysed with different collocation criteria to examine the results from different experiments. Four experiments with differing quality control were defined. The details of these experiments and the derived uncertainties are shown in Table 3. A further two experiments were defined for different time criteria and region, although these have a lower number of collocations.

Experiment name	Criteria	IASI SST error (K)	AVHRR SST error (K)	Drifting buoy SST error (K)	Number of collocations
1. Stdev_noql_qc	Stdev_check NO QL3_check	0.33	0.17	0.20	1139
2. No_qc	NO stdev_check NO QL3_check	0.36	0.19	0.23	1442
3. Stdev_ql_qc	Stdev_check QL3_check	0.34	0.16	0.21	503
4. av_stdev_noql_qc	Averaged AVHRR SST Stdev_check No QL3_check	0.38	0.13	0.21	1681
5. Stdev_noql_qc_1hr	Stdev_check NO QL3_check 1 hour between IASI and buoy	0.34	0.19	0.17	455
6. Nostdev_ql_qc_so	NO Stdev_check QL3_check Southern Ocean region	0.37	0.15	0.15	171

Table 3: Estimated standard deviation of error for IASI, AVHRR and drifting buoy SSTs for April-September 2010

The uncertainties for each observation type are quite consistent over the six experiments, leading to the conclusion that the errors between the observations are uncorrelated and the assumption made is valid. The standard deviation of error for IASI varies between 0.33 K and 0.38 K; for AVHRR between 0.13 K and 0.19 K; for drifting buoys between 0.15 K and 0.23 K. The values for experiment 1, which has a large number of collocations but also retains some further quality control, are: for IASI 0.33 K, for AVHRR 0.17 K, and for drifting buoys 0.20 K. The uncertainty in the drifting buoy supports the results found in [RD 11].

Figure 8 shows the Global monthly standard deviation of errors from three-way collocations for April to September 2010. The errors for the lowest quality level (2) were generally the highest, with some month-to-month variability.

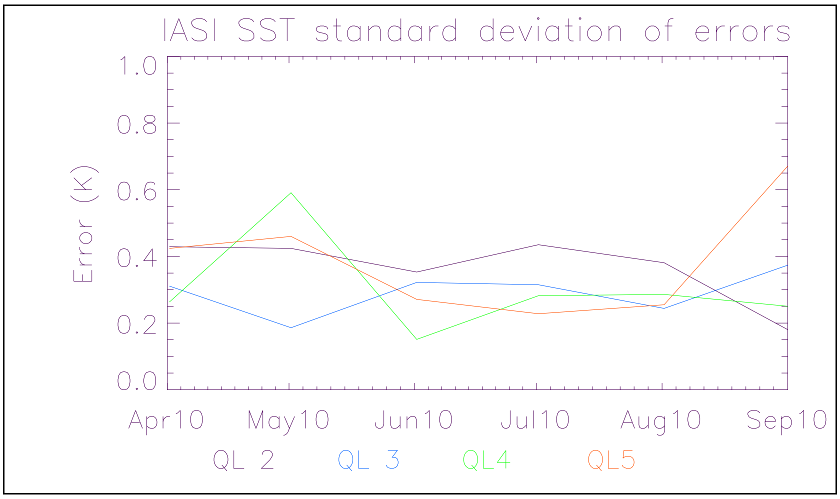

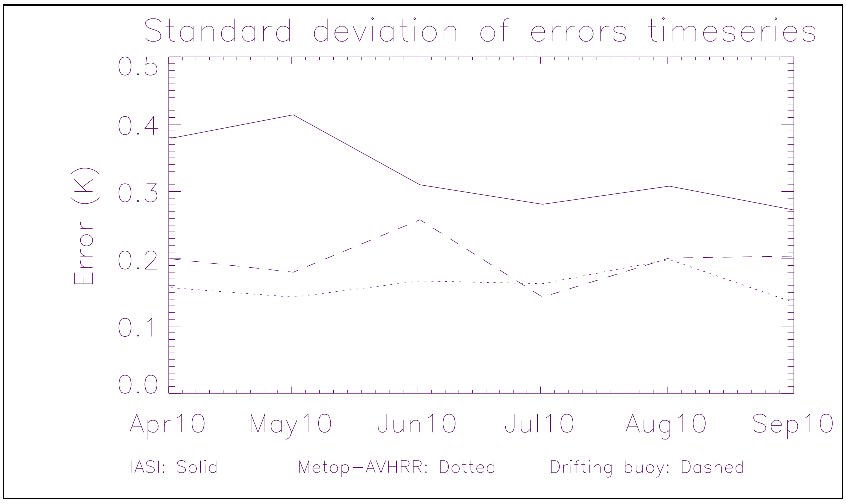

Figure 8: a) (top) Global monthly standard deviation of errors from three-way collocations for April to September 2010; b) (lower) Global monthly standard deviation of errors from three-way collocations for April to September 2010 for IASI (solid), AVHRR (dotted), and drifting buoys (dashed)

A separate analysis of three-way errors (with non-3-sigma statistics) using AATSR (L3), Metop/AVHRR (L3) and IASI L2 SST (all quality levels) for November 2008 showed IASI to have a standard deviation of error equal to 0.48 K; for AVHRR the error is 0.28 K, and for AATSR the error is 0.22 K. Tests where the quality control conditions were varied showed that the errors between the observations were uncorrelated. The IASI L2 SST data used came direct from the PPF, rather than from the L2Pcore product. These errors are consistent with the errors derived for IASI and AVHRR using the IASI L2Pcore data, and also with [RD 11] for AATSR uncertainties.

3.3 Point to Area Uncertainty Contributions

In order to examine the uncertainties involved in the retrieval of SST from space, traditional methods involve the use of *in situ* observations. The error in drifting buoys has been shown to be approx 0.2 K in this report and [RD 11], which approaches or exceeds the error in the satellite SST retrieval. Drifting buoy observations, used in this validation exercise, are representative of a point observation of the ocean surface. As the satellite SSTs represent a temperature over a spatial field of view, there is a geophysical error involved in collocating these two different observation types. The three-way error analysis method assumes that this error arising from the covariances between the observations because of this representativity error is negligible. As the IASI MMD contains information of a 21x21 AVHRR pixel box over the larger IASI IFOV, we are able to estimate the error contribution from representativity error and validate whether the assumptions made are valid.

The AVHRR data contained within the OSI-SAF MDB also contain SST information around a 21x21 box around the central pixel, and provides information on the standard deviation of AVHRR SSTs within that box. Therefore the IASI MMD is an ideal dataset to examine errors in the buoy observations from point-to-area measurement contributions. Figure 9 shows an example of how the AVHRR SST can vary within the 21x21 pixel box. As the radius of the IASI IFOV is approximately 11 times that of AVHRR, the AVHRR 21x21 box can be used as a good approximation for comparing spatial SSTs directly.

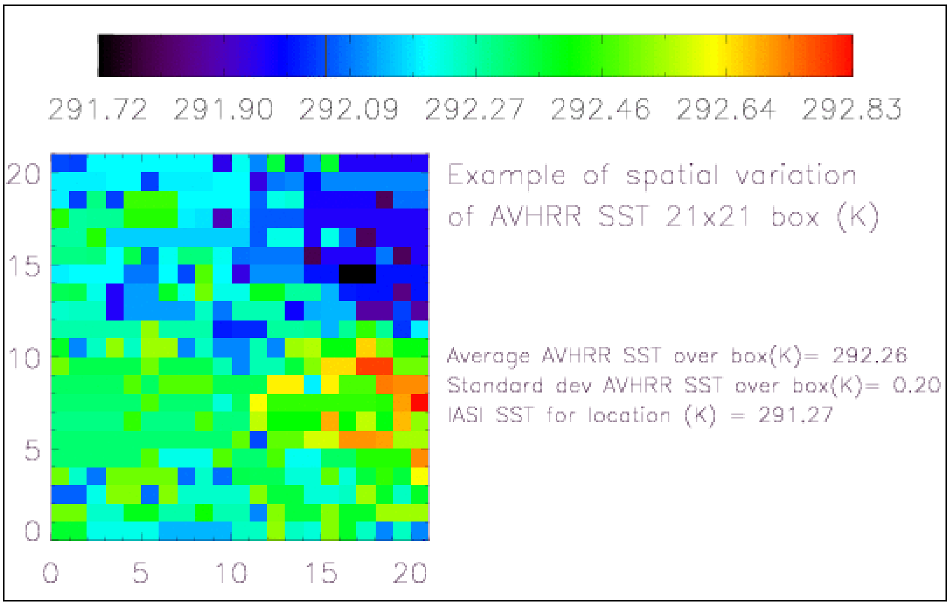

Figure 9: Example of AVHRR SST variation over a 21x21 box

The known quantity of the standard deviation of the AVHRR SSTs over the 21x21 grid box can be added and subtracted to the couplets of IASI minus buoy, AVHRR minus IASI, and buoy minus AVHRR differences at observation level, to give a maximum and minimum range of mean observation differences. These are then fed into the estimation of standard deviation of errors, to give a range of uncertainties according to the range of the standard deviations. The range can be examined to infer the uncertainty contribution from the spatial-to-point approximations. These errors range from ±0.004 K to ±0.012 K, and are shown in Table 4. They are dependent on the spatial variability of the ocean. This supports the assumption that the covariances between the observations from representativity error are negligible.

Experiment 1	**Error IASI (K)**	**Error AVHRR (K)**	**Error drifting buoy (K)**
Mean (as reported in Table 3)	0.393	0.188	0.280
Max	0.397	0.186	0.275
Min	0.389	0.210	0.287
Variation	±0.004	±0.012	±0.006

Table 4: Standard deviation of error (no 3-sigma standard deviation tests) for IASI, AVHRR and drifting buoy observations, given the variation of AVHRR standard deviation for 1 April to 30 September 2010

It is possible to compare the point AVHRR minus IASI statistics with averaged AVHRR (over box) minus IASI statistics. For the point differences the mean difference is 0.43 K (standard deviation 0.38 K), whilst the averaged AVHRR–IASI mean difference is 0.48 K (standard deviation 0.41 K) for 777 collocations. Therefore, both the bias and the standard deviation increase for the averaged AVHRR SST statistics.

3.4 Regional Statistics

Analyses of regional areas have been compiled based upon the OSI-SAF region mask. Table 5 shows the statistics of comparisons of the three observation types. Only regions where a significant number of matchups occurred have been presented. The quality control criteria in the matchup process are more relaxed for the regional analyses (see Table 1) in order to keep a useable quantity of matchups. Therefore the global statistics have also been presented again in Table 5, with the same criteria as the regional analyses. The standard deviations of the differences are all less than 0.5 K, except for in the North-East Pacific where the standard deviation is 0.83 K for both differences, although there are a low number of collocations in this region. IASI is shown to have a cool bias with respect to AVHRR and *in situ* observations for all the regions, ranging from the lowest biases in the North-East Atlantic and North-East Pacific to the highest biases in the North-West Atlantic. IASI SSTs in the North Central Pacific region have a warm bias of 0.19 K compared to buoy SSTs. Figure 10 shows histograms (not including 3-sigma test) of IASI minus buoy SST differences for the six regions. A residual cool tail is shown on all the histograms.

Region	IASI–buoy mean diff. (K)	IASI–buoy st. dev. (K)	AVHRR–IASI mean diff. (K)	AVHRR–IASI st. dev. (K)	Number of collocations
Global	-0.40	0.46	0.40	0.43	1698
Arctic Ocean	-0.42	0.48	0.43	0.45	770
Southern Ocean	-0.34	0.40	0.38	0.40	171
North-West Atlantic	-0.47	0.37	0.41	0.40	120
North-East Atlantic	-0.23	0.42	0.17	0.40	26
North-East Pacific	-0.22	0.83	0.12	0.83	16
South Equator Pacific	-0.42	0.44	0.40	0.43	14
North Central Pacific	0.19	0.32	-0.07	0.38	51
South-East Pacific	-0.42	0.46	0.50	0.39	52

Table 5: Regional SST difference statistics (including 3-sigma test) for 1 April to 30 September 2010

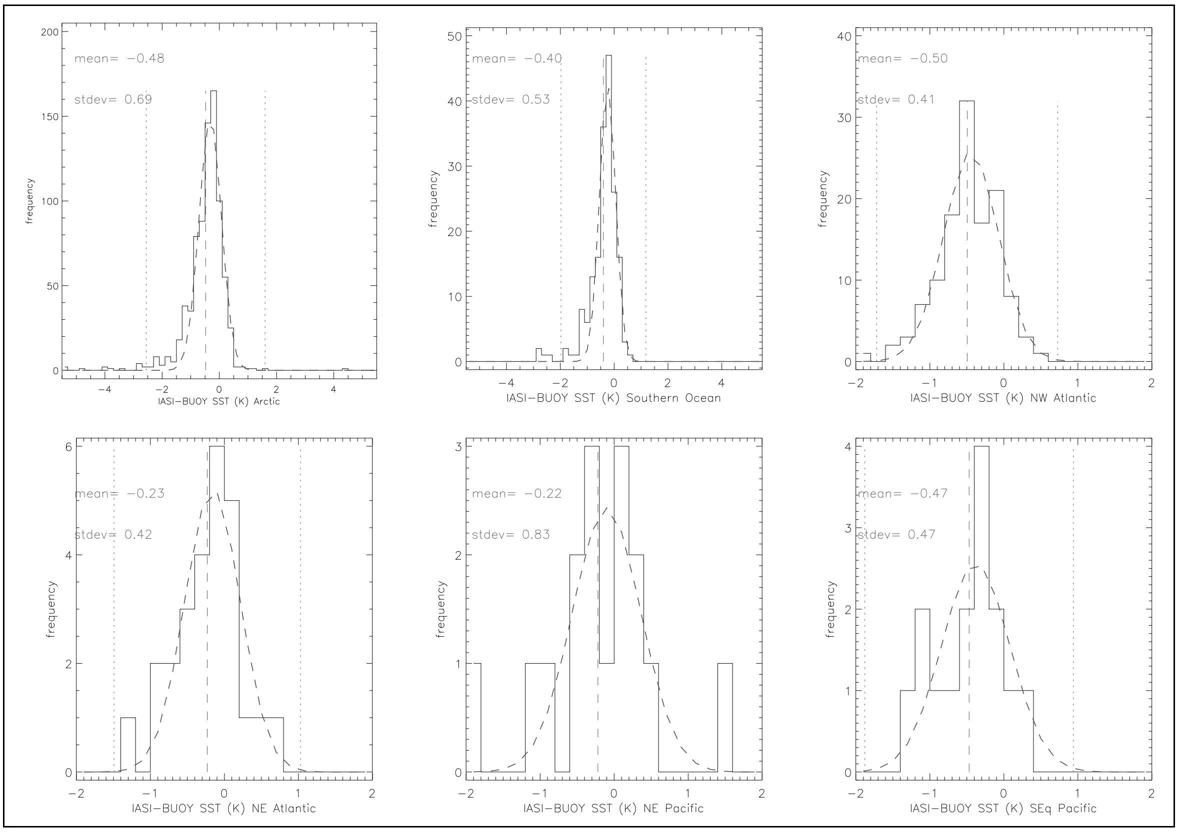

Figure 10: Histograms of IASI minus buoy differences for 1 April to 30 September 2010 for six regions

3.5 Cloud Investigations

It is possible that some residual cloud-contaminated pixels remain in the IASI SST data, which are contributing to the IASI SST cool bias. This section examines cloud information provided in the OSI-SAF MDB more closely to understand the relationship between the amount of cloud in the IASI IFOV and the biases.

The first set of figures (Figure 11, Figure 12, Figure 13) shows IASI minus buoy SST differences versus data variables which give an indication of cloud conditions within the IASI IFOV. The AVHRR 21x21 box gives further information on SST variability and cloud masks within the IASI IFOV. Figure 11 shows that there are only weak correlations between IASI minus buoy differences versus box rate (number of clear pixels as a percentage) and AVHRR standard deviation. The binned graphs (Figure 13) show that as box rate increases (so there are more AVHRR observations in the IASI IFOV meaning there is less cloud) then the IASI cool bias decreases. Figure 12 shows no correlations with the OSI-SAF cloud-mask indicator and distance-from-cloud information.

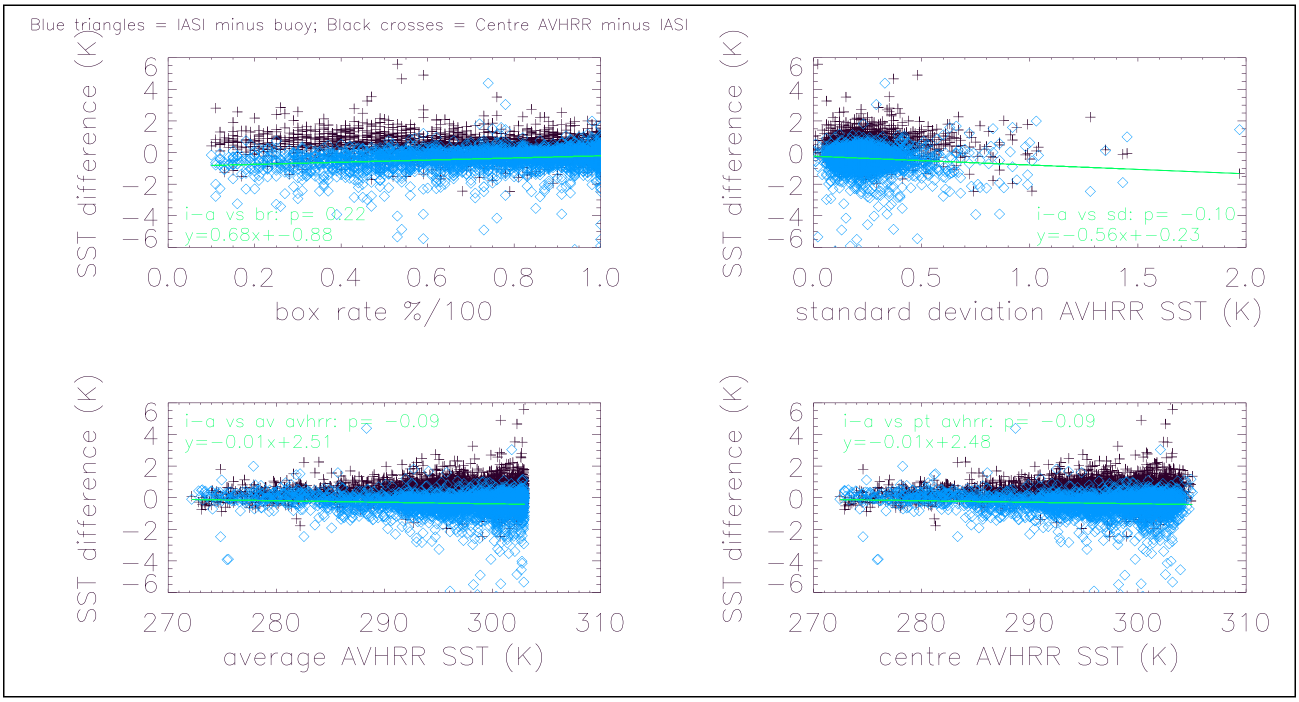

Figure 11: IASI minus buoy SST differences versus box-rate; standard deviation of AVHRR SST within 21x21 box; average AVHRR SST over 21x21 box; and centre AVHRR SST, for 1 April to 30 September 2010

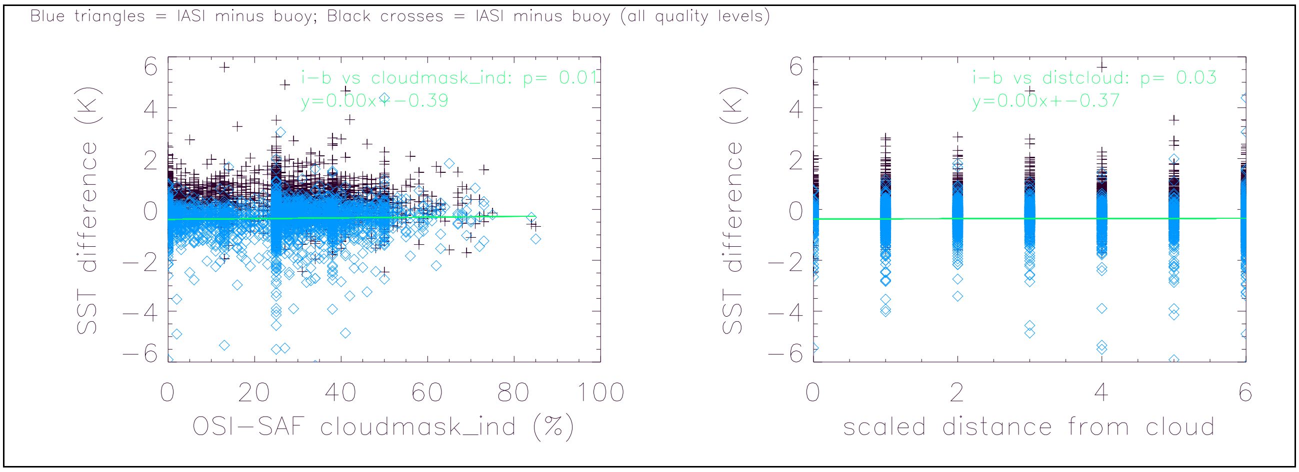

Figure 12: IASI minus buoy SST differences versus OSI-SAF cloud-mask indicator; and scaled distance from cloud (6 very far), for 1 April to 30 September 2010

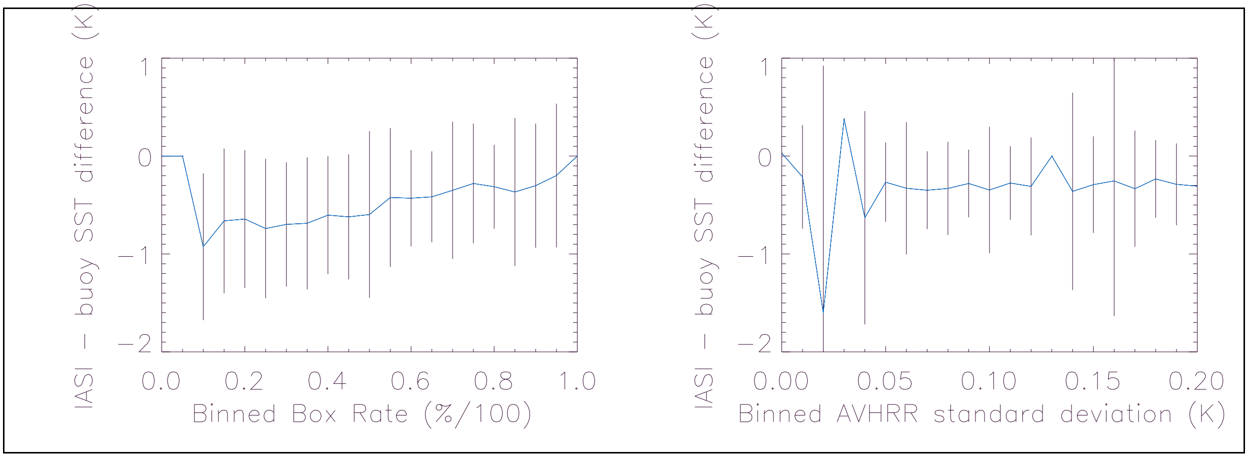

Figure 13: IASI minus buoy SST differences versus binned box-rate; binned standard deviation of AVHRR SST within 21x21 box, for 1 April to 30 September 2010

Figure 14 and Figure 15 show IASI minus buoy SST differences versus latitude and versus wind-speed information. The IASI bias does vary with latitude, as shown from the SSES derivations in Section 2.2. The larger biases are in the tropics where the water vapour loadings are higher. The binned wind speed graph in Figure 15 shows how at night-time (blue curve) the IASI minus buoy difference varies with wind speed, with the larger cooler IASI SSTs at the lower wind speeds due to the skin effect [RD 15, RD 16]. During day-time (green curve) the curve flattens due to diurnal warming effects changing the structure of the ocean surface layer. Although the IASI SSTs have been converted to a ‘sub-skin’ SST for these plots, due to the limitations of the 0.17 K conversion, the IASI–buoy differences do indicate standard ‘skin to bulk’ variations with wind speed [RD 10, RD 15, RD 17].

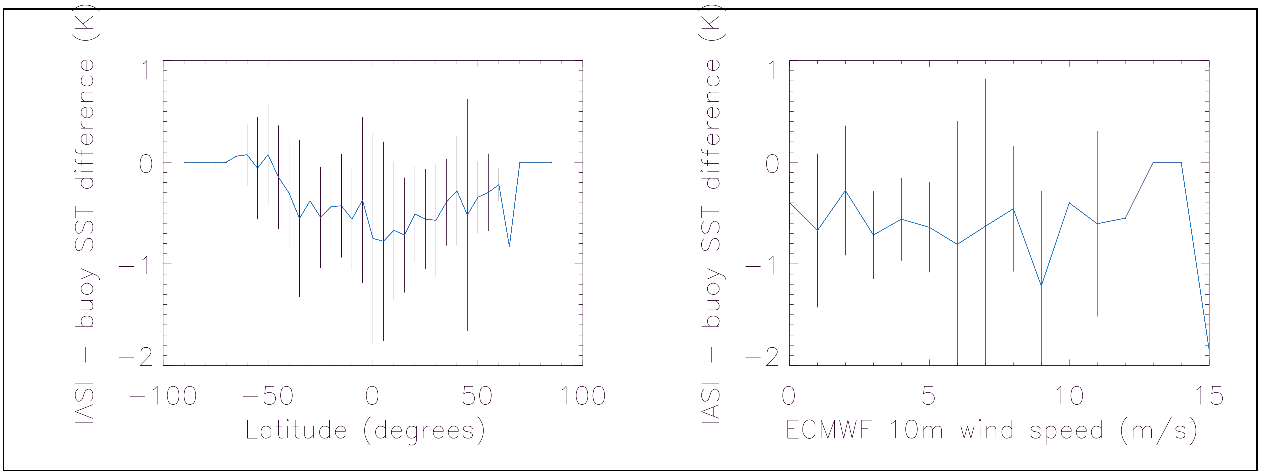

Figure 14: IASI minus buoy SST differences versus binned latitude; binned ECMWF wind speed (ingested independently), for 1 April to 30 September 2010

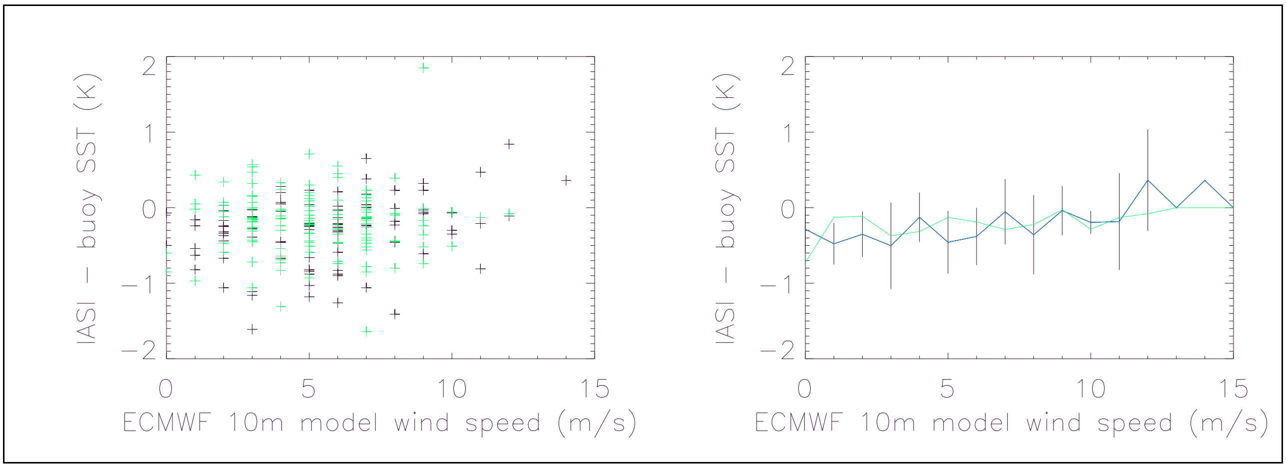

Figure 15: IASI minus buoy SST differences versus ECMWF 10m wind speed provided in IASI L2Pcore product; binned ECMWF wind speed (blue=night, green=day) for October 2010

Figure 16 shows the variation of IASI SST bias with satellite zenith angle. Towards the edge of the scan, where the satellite zenith angle is greater than 40 degrees, the bias increases. This slight dependence should be corrected with future updates of the IASI SST retrieval algorithms in the L2 PPF.

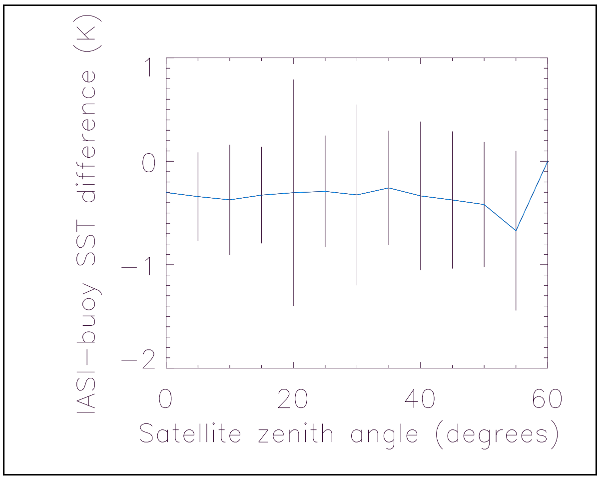

Figure 16: IASI minus buoy SST differences versus satellite zenith angle for April to September 2010

Figure 17 displays global maps of 5-degree averaged gridded values of IASI–buoy SST differences; AVHRR–IASI SST differences; AVHRR standard deviation over a 21x21 box; and box rate. There is no obvious pattern between the IASI biases with the box rate and standard deviation maps. However, the locations of the most extreme values where the IASI SSTs are very cool compared to buoys (>2 K) relate to pixels where the box rates are low (<0.5) and cases can be seen in the mid-Atlantic, equatorial Pacific and Indonesian regions. It is therefore possible that the very cool IASI SST grid points are affected by cloud contamination in these highly cloudy regions. The IASI biases when using the averaged AVHRR SSTs are lower in these pixel locations, which could mean that AVHRR is also affected by residual cloud contamination in the wider box, or there is a large spatial variability of SST within the box (which could cause a low box rate value as the cloud-masking contains spatial variability tests).

The AVHRR standard deviation maps show no correlations with the largest IASI–buoy difference locations and do not display any relationships to cloud amount. However, in a few cases where the standard deviations are greater than 0.5 K, the IASI SST can be greater than buoys by more than 1 K, possibly due to area-to-point errors.

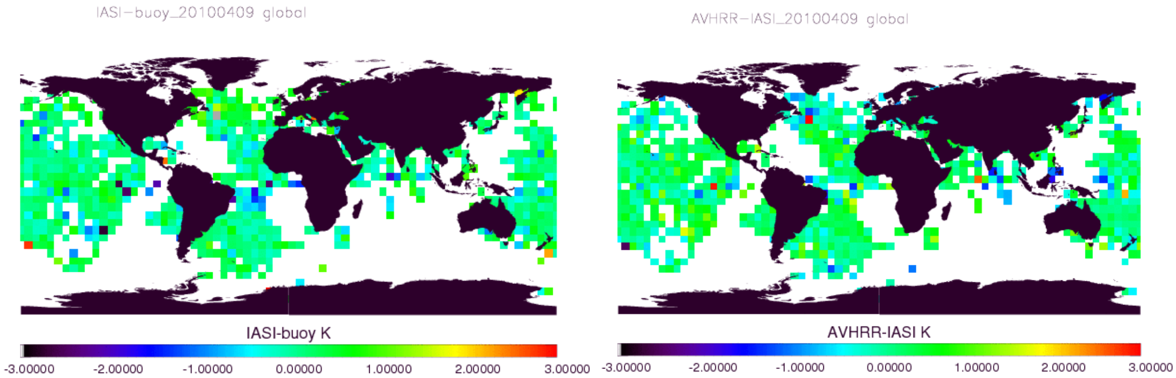

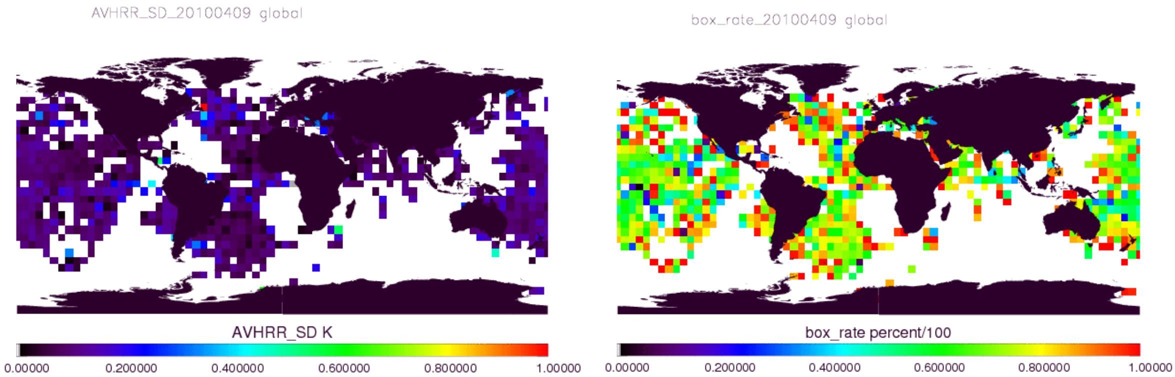

Figure 17: Five-degree gridded global maps of IASI minus buoy SST differences; AVHRR minus IASI; standard deviation of AVHRR within 21x21 grid box; and AVHRR box-rate for 1 April to 30 September 2010

Figure 18 shows firstly a global map of five-degree gridded SST differences for buoy minus AVHRR; followed by the standard deviation over the 5-degree grids for IASI minus buoy, AVHRR minus IASI, and buoy minus AVHRR differences, over the period April to September 2010. The standard deviation plots show that in regions where there are no significant large biases with respect to drifting buoy data, so therefore no problems from residual cloud or aerosol contamination, the standard deviations for IASI compared to drifting buoys is slightly lower than for AVHRR. This behaviour can be seen in the South Atlantic, West Pacific, the mid-Atlantic, and off the west coast of north America. The bias maps in Figure 17 and Figure 18 show large differences in some isolated locations for both IASI and AVHRR SSTs compared to drifting buoy SSTs. These locations are sometimes different. In particular, AVHRR is biased cool by up to 2 K around the Malvinas current and off the South African coast, but in these regions IASI is comparable to the drifting buoy SST. There are also locations where the IASI SST is cool compared to drifting buoy SSTs, but AVHRR SSTs are more comparable, for example, in the Indian Ocean. There is also a large region in the south-east Pacific where AVHRR is cool compared to drifting buoys, but IASI SSTs are more comparable, except for more isolated grid points. Therefore, these results show that IASI SSTs are a complementary source of data to AVHRR SSTs, giving benefits in regions where AVHRR show large biases. In regions where the IASI SSTs are performing well and are unaffected by cloud issues, the standard deviations are very slightly lower compared to drifting buoys than AVHRR SSTs.

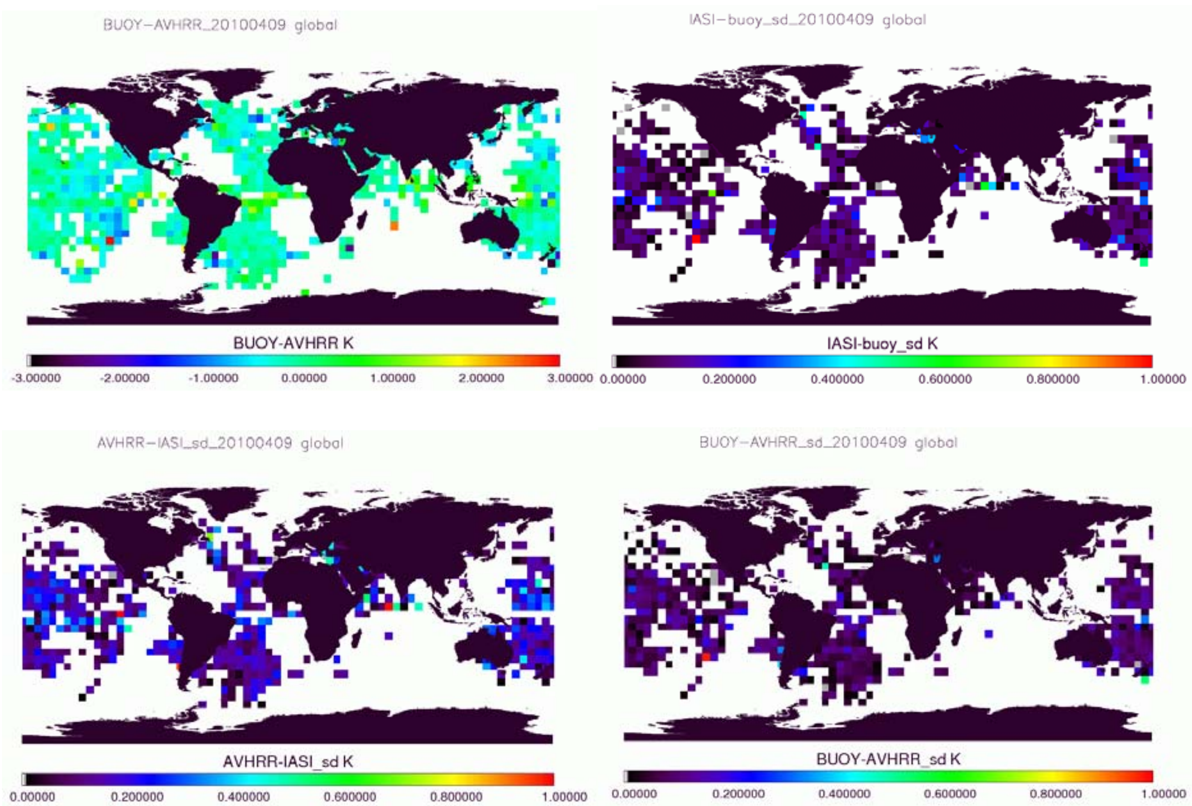

Figure 18: Five-degree gridded global maps of buoy–AVHRR SST differences; standard deviation of IASI–buoy SST differences; standard deviation of AVHRR–IASI SST differences; standard deviation of buoy–AVHRR SST differences for 1 April to 30 September 2010

4 CONFORMITY OF OPERATIONAL PRODUCT IMPLEMENTATION

4.1 Comparison of netCDF Format Files

Checks were performed to check the netCDF file format between the prototype and operational implementation versions. The following checks were performed:

- The use of ncdump to check that the global_attributes conform to each other.
- The use of ncdump to check that the variable_attributes conform to each other.
- The method of computation of integrated water vapour was compared and re-coded to check the validity of the method, and comparisons were made against ECMWF water vapour products to confirm the units.

4.2 Verification of SSES Application

Further analyses of the application of the quality levels and the SSES within the operational implementation compared to the prototype files were performed. Data for 15 December 2010, 19 January 2011 and 1 February 2011 were analysed. Plots were produced for quality_level, sses_bias, sses_standard_deviation, sea_surface_temperature for quality_level 0 to 5, and sea_surface_temperature for quality_level 2 to 5. Figure 19 shows example plots for quality_level, SSES and sea_surface_temperature for 1 February 2011.

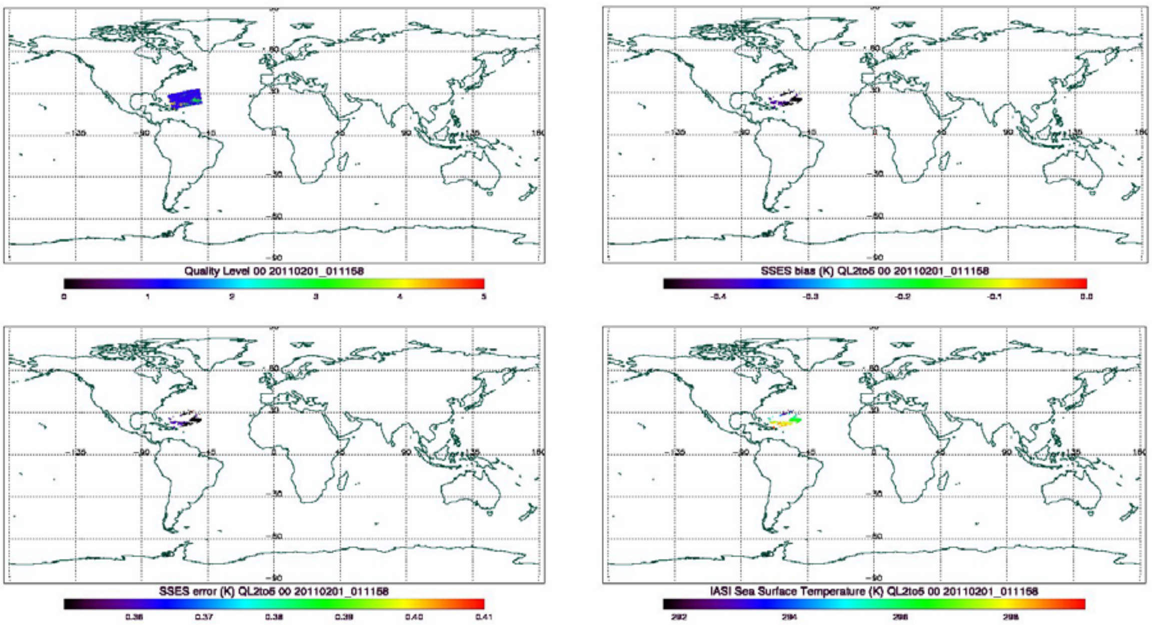

Figure 19: Quality_level, sses_bias, sses_standard_deviation, and sea_surface_temperature (quality_level 2 to 5) for one granule on 1 February 2011

The distribution of quality_level, sses_bias, sses_standard_deviation and sea_surface_temperature for the prototype implementation are confirmed as being within the expected ranges.

5 CONCLUSIONS AND WAY FORWARD

IASI L2Pcore SSTs have been produced routinely at EUMETSAT since March 2010. A IASI MMD is routinely produced using collocations with the OSI-SAF Metop/AVHRR MDB. Comparisons with *in situ* SST and Metop-AVHRR SST observations show the IASI SSTs to have a slight cool bias of around 0.4 K. Standard deviations of the differences are around 0.4 K, supporting the conclusion that the IASI SSTs are of good quality. These results have been compiled with night-time only data to remove the effect of diurnal variations during the day-time. Day-time analyses show the IASI SSTs warming by 0.15 K, reducing the cool bias.

A three-way error analysis shows the uncertainty in the IASI SST observations to be 0.33 K (ranging from 0.33 K to 0.38 K), for AVHRR SSTs to be 0.17 K (ranging from 0.13 K to 0.19 K), and for drifting buoy SSTs to be 0.20 K (ranging from 0.15 K to 0.23 K). Tests show that the errors between the observations are uncorrelated, therefore these uncertainty estimates are valid. This analysis shows the IASI SSTs to be of good quality. The error in the AVHRR is lower than that of the drifting buoys and more comparable to the AATSR error derived in [RD 11]. The error in the drifting buoys is consistent with that derived in [RD 11].

The cool bias in the IASI SST observations may arise from residual cloud contamination. Global maps of the differences indicate the largest deviations to be off the west coast of Africa and in the Arabian Sea, supporting the conclusion that the presence of aerosol contributes to a cooling in the IASI SST observations. A relationship is observed where the IASI cool bias (with respect to *in situ* observations) decreases as the AVHRR box rate increases, i.e. there are more clear AVHRR observations in the IASI IFOV. This suggests that residual cloud contamination may be influencing the IASI SST observations.

In regions where IASI SSTs do not appear to be affected by large biases with respect to drifting buoys and thus potential cloud contamination, then the standard deviations of comparisons with buoys are very slightly less than for AVHRR SSTs. The IASI SSTs have been shown to have the potential for the improvement of derived SST in these regions. In addition, in some locations where AVHRR display large biases with respect to drifting buoys, the IASI SSTs are closer to the buoy SSTs. Therefore, the results show that IASI SSTs are a complementary source of SST data to AVHRR SSTs, with potential benefits over large regions.

The contribution of errors arising from comparing SST observations at a point to those arising from an area has been estimated by varying the observation differences according to the spatial variation of AVHRR over the IASI IFOV within the three-way error analysis method. The point-to-area error contribution was estimated at being approximately ±0.01 K (ranging from ±0.004 K to ±0.012 K). This supports the assumption that the covariances between the observations from representativity error are negligible.

Regional analysis of the statistics showed that the standard deviations of the differences were all less than 0.5 K where there were a significant number of collocations. A IASI cool bias was observed for all regions except one.

Overall, the IASI SSTs have been shown to be of good quality. Improvements to the IASI SST retrieval scheme and the cloud detection are currently under development, where issues such as the slight cool bias and scan edge effects will be tackled. SSTs from the IASI instrument are an important contribution to the global distribution of SST observations, and with similar instruments planned for post-EPS and MTG, will provide a good quality, long-term, consistent dataset for modelling, analyses, inter-comparisons, validation/calibration, and climate purposes.

6 ACKNOWLEDGEMENTS

The Metop/AVHRR *in-situ* matchup database was provided by the OSI-SAF. AVHRR L3P SSTs were also obtained from the OSI-SAF. Sonia Pere and Anne Marsouin, from CMS/Meteo-France, provided the buoy black list files and the region masks. The monthly NSIPP SST climatology based on Pathfinder (v4.1) from 1985-1997 was used to evaluate the quality indicator thresholds. AATSR L3 data were obtained from Ifremer www.ifremer.fr.

7 REFERENCES

RD 1. Klaes, K.D., M. Cohen, Y. Buhler, P. Schlüssel, R. Munro, A. Von Engeln, E. O'Clérigh, H. Bonekamp, J. Ackermann, and J. Schmetz, An Introduction to the EUMETSAT Polar system. *Bull. Amer. Meteor. Soc.*, **88**, 1085–1096, 2007.

RD 2. IASI Level 2 Product Format Specification, EUM.EPS.MIS.SPE.980760.

RD 3. IASI L2 Surface Temperature PPF v5 Validation Results, EUM/MET/TEN/10/0188, v1, 1 June 2010.

RD 4. The recommended GHRSST Data Specification Revision 2.0, https://www.ghrsst.org/documents/q/category/gds-documents/operational/GDS2.0_TechnicalSpecifications_v2.0.pdf

RD 5. EUMETSAT satellite programmes overview http://www.eumetsat.int/Home/Main/Satellites/SatelliteProgrammesOverview/index.htm?l=en

RD 6. Alien, M.R., C.T. Mutlow, G.M.C. Blumberg, J.R. Christy, R.T. McNider, and D.T. Llewellyn-Jones, Global change detection. *Nature*, **370,** 1–82, 1994.

RD 7. Minnett, P., A numerical study of the effects of anomalous North Atlantic atmospheric conditions on the infrared measurement of sea surface temperature from space, *J. Geophysical Research*, 91, C7, 1986.

RD 8. Casey, K.S., and P. Cornillon, A Comparison of Satellite and In-Situ Based Sea Surface Temperature Climatologies, *Journal of Climate*, Vol. 12, No. 6, pp 1848-186, 1999.

RD 9. Le Borgne, P., G. Legendre, A. Marsouin, and S. Pere, Operational SST retrieval from METOP/AVHRR validation report, *Ocean and Sea-Ice SAF CDOP report*, Version 2.0, July 2008.

RD 10. Centre-de-Météorologie-Spatiale (CMS) buoy black list available from Sonia Pere CMS/Meteo-France (sonia.pere@meteo.fr).

RD 11. Donlon, C.J., P.J. Minnett, C. Gentemann, T.J. Nightingale, I.J. Barton, B. Ward, and M.J. Murray, Toward improved validation of satellite sea surface skin temperature measurements for climate research. *J. Climate*, **15,** 353–369, 2002.

RD 12. O'Carroll, A.G., R.W. Saunders and J.R. Eyre, Three-Way Error Analysis between AATSR, AMSR-E, and In Situ Sea Surface Temperature Observations, *J. Atmos. Oceanic Tech.*, Vol. 25, No. 7, p1197, 2008.

RD 13. Stoffelen, A., Toward the true near-surface wind speed: Error modeling and calibration using triple collocation, *J. Geophys. Res*., **103** (C4), 7755–7766, 1998.

RD 14. Janssen, P.A., S. Abdalla, H. Hersbach, and J.R. Bidlot, Error Estimation of Buoy, Satellite, and Model Wave Height Data, *Journ. Atmos. Oceanic. Tech.*, **24**, No. 9, pp 1665-1677.

RD 15. Byongjun, H., and T. Lavergne, Triple comparison of OSI SAF low resolution sea ice drift products, SAF/OSI/CDOP/met.no/SCI/RP/152, September 2010.

RD 16. Horrocks, L.A., B. Candy, T. Nightingale, R.W. Saunders, A.G. O'Carroll, and A.R. Harris, Parameterizations of the ocean skin effect and implications for satellite-based measurement of sea-surface temperature, *J. Geophys. Res.*, 3096, 2003.

RD 17. Fairall, C.W., E.F. Bradley, J.S. Godfrey, G.A. Wick, J.B. Edson, and G.S. Young, Cool-skin and warm-layer effects on sea surface temperature, *J. Geophys. Res.*, **101,** 1295–1308.

RD 18. Schluessel, P., W.J. Emery, H. Grassl, and T. Mammen, On the bulk-skin temperature difference and its impact on satellite remote sensing of sea surface temperature, *J. Geophys. Res.*, 95, C8, *13341-13356*, 1990.

APPENDIX A ACRONYMS AND ABBREVIATIONS

AATSR	Advanced Along-Track Scanning Radiometer (ENVISAT)
ASCAT	Advanced SCATterometer
ATOVS	The Advanced TIROS Operational Vertical Sounder
AVHRR	Advanced Very High Resolution Radiometer
ECMWF	European Centre for Medium-Range Weather Forecasts
EO	Earth Observation
EPS	EUMETSAT Polar System
EUMETSAT	European Organisation for the Exploitation of Meteorological Satellites (Darmstadt, Germany)
FCDR	Fundamental Climate Data Record
GDS	GHRSST Data Specification
GHRSST	Group for High Resolution Sea Surface Temperature
GOME	Global Ozone Monitoring Experiment
GRAS	Global Navigation Satellite System Receiver for Atmospheric Sounding
IASI	Infrared Atmospheric Sounding Interferometer
IFOV	Instantaneous Field Of View
IWV	Integrated water vapour
L2	Level-2
L2P	Level-2 Pre-processed
Metop	METeorological OPerational (satellite)
MMD	Multi-Matchup Dataset
NetCDF	Network Common Data Form
NSIPP	NASA Seasonal-Interannual Prediction Project
OIS	Operational Internet Service
OSI SAF	Ocean and Sea Ice Satellite Application Facility
PPF	Product Processing Facility
SSES	Single Sensor Error Statistic
SST	Sea Surface Temperature